PAPER • OPEN ACCESS

Manufacturing and characterisation of 3D printed thermoplastic morphing skins

To cite this article: Rafael M Heeb *et al* 2022 *Smart Mater. Struct.* **31** 085007

View the article online for updates and enhancements.

Manufacturing and characterisation of 3D printed thermoplastic morphing skins

Rafael M Heeb[*] ⓘ **, Michael Dicker and Benjamin K S Woods**

University of Bristol, Faculty of Engineering, Queen's Building, University Walk, Bristol BS8 1TR, United Kingdom

E-mail: rafael.heeb@bristol.ac.uk

CrossMark

Abstract

Morphing aircraft are one promising solution to reducing the aviation industry's environmental impact because they can make aircraft more aerodynamically efficient, thereby reducing greenhouse gas emissions. The design of morphing skins is inherently challenging due to the competing design constraints of needing to be stiff out-of-plane to resist pressure loads while being compliant in-plane to minimise actuation energy. Previous work by these authors introduced the novel concept of Geometrically Anisotropic Thermoplastic Rubber (GATOR) morphing skins that take advantage of multi-material 3D printing and structural scaling laws to allow for better compromises between these competing design constraints. In this work, multi material Fused Filament Fabrication methods were used to 3D print the proposed GATOR sandwich panels from two different stiffnesses of thermoplastic polyurethane to demonstrate the manufacturing process and experimentally quantify the performance of some simple embodiments of the GATOR concept. The panels were mechanically tested to determine their flexural and extensional stiffnesses. Results show that the panels can be extended to a stretch ratio of $\lambda = 1.6$ with a linear response at low stretch ratios. The results from the flexural experiments show that the flexible face sheets are capable of withstanding some compression before buckling, which results in a linear behaviour at small forces. These results show the promise of the GATOR skin concept and motivate future development of designs that further exploit the underlying principles of the concept.

Keywords: morphing, smart structures, multi-material, 3D printing, thermoplastic polyurethanes

(Some figures may appear in colour only in the online journal)

1. Introduction

Despite the fact that the aviation industry today only accounts for roughly 2% of global emissions, that is still 915 million tons of CO_2 [1]. What is worse, the industry is forecasted to see significant continued emissions growth as other industries have realised significant reductions. Aircraft emissions can be significantly reduced by decreasing drag and therefore thrust required from the propulsion system, which in return will lower fuel burn.

Control surfaces such as ailerons and flaps are a significant contributor to vehicle drag, both during use and when stowed, due to spanwise and chordwise gaps, which create shed vorticity and increase profile drag. The proposed solution to reducing control surface drag is to replace traditional

---

[*] Author to whom any correspondence should be addressed.

hinged control surfaces with morphing devices. The smooth and continuous shape adaptations [2, 3] provided by morphing promise to reduce vehicle drag through a number of physical mechanisms, including delayed flow separation, reduced shed vorticity, and lower induced drag through continuously optimised spanwise lift distributions.

Flight design parameters such as the lift over drag (L/D) can also be improved using morphing devices, resulting in an increased loiter time and cruise distance. This can be achieved with a hinged wing tip seen on the Boeing 777x or the Airbus Albatross, [4] which can be replaced with a flexible morphing wing section. An increased L/D can achieve the same effect with a span morphing device that telescopically extends in the spine wise direction.

One of the primary reasons morphing technologies have not been widely adopted is the lack of suitable skin technologies. Morphing skins are beholden to directly competing design requirements—they need to be highly flexible in-plane to keep the actuation energy manageable while also being stiff enough out-of-plane to withstand the aerodynamic loading with acceptably low deformation [3, 5]. Above all, the structure must be light and robust enough to be utilised within an aerospace environment. Research has shown that this problem cannot be solved with traditional aerostructural solutions, and so instead, novel solutions are needed.

Previous work by these authors introduced the novel concept of Geometrically Anisotropic ThermOplastic Rubber (GATOR) [6] skins as a possible solution to the morphing skin problem. The GATOR skin concept combines three fundamental design principles to create scalable morphing skins with highly tailorable mechanical properties that can partially decouple the in-plane stiffness from the out-of-plane stiffness, allowing a better compromise between these competing constraints. These three design principles are as follows [6]:

(a) Use of 3D printed thermoplastic polyurethane (TPU) elastomers to provide material compliance and manufacturing freedom.
(b) Making components from multiple stiffnesses of TPU, with careful control of where the different stiffness are used.
(c) Exploitation of geometric scaling laws and anisotropy to better balance in-plane and out-of-plane mechanical properties.

The GATOR skin concept is used to manufacture a morphing sandwich panel skin, using TPU elastomers and Fused Filament Fabrication (FFF) methods these authors proposed [6]. As shown in figure 2, a zero Poisson's ratio cellular core is placed between two skin sheets as shown in figure 1. The core is printed from a stiffer grade of TPU and can undergo large deformations due to its geometry. The flexible skin sheets are printed from a softer TPU, achieving the same levels of deformation as the core but through direct material strain. Together these components ensure a smooth, continuous, and gap free aerodynamic surface over a wide range of achievable morphed shapes. Furthermore, a multi-material FFF printer allows the core to be printed directly onto the flexible face
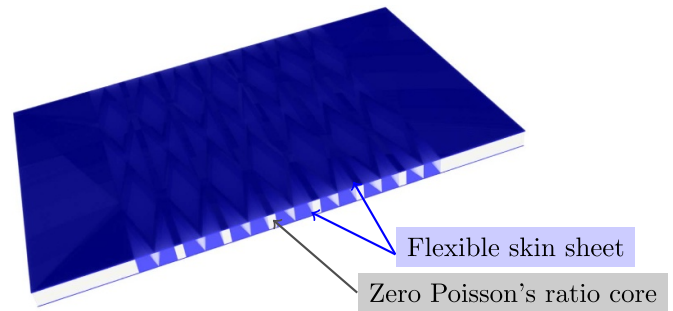

Figure 1. Fully assembled test panel.

sheets. The similar chemical formulations of the two TPUs allow for creating a strong bond during printing through thermoplastic fusion without using adhesives. This 3D printing strategy has already been successfully implemented by these authors in printing stringers and mounting tabs from a stiff TPU formulation onto a softer phase membrane for a FishBAC morphing skin [7].

At this point, it is worth looking into how GATOR design principles can be used to solve the above stated problem. This is best done by looking at the core and skin sheet in isolation to determine their individual merits and how they can be further tailored to enhance their respective properties for the use in GATOR morphing skins.

The purpose of the face sheets is to provide an airtight surface that maintains the desired airfoil shape under aerodynamic loading. Elastomers are attractive here because of their ability to achieve high direct strain levels with moderate axial stiffness. In this work, we focus on TPU's, such as NinjaFlex®, Filaflex® and Polyflex® which can withstand strains up to 100% [8–11] without yielding. This makes them ideal materials for use in skin membranes. The challenge with single material skin sheets—which have a very low out-of-plain stiffness—is to find a good balance between keeping the in-plane stiffness low whilst providing enough out-of-plane stiffness to resist the pressure loading. The out-of-plane stiffness can be increased by pre-stretching the face sheet or increasing the skin thickness (or some combination of both). These approaches will result in higher required in-plane actuation forces as a trade-off. Alternatively, the face sheet stiffness can be tailored by strategically adding fibre reinforcement, which can be directly printed into it, either by using a stiffer formulation TPU as the fibre or indeed by using fibre reinforced TPUs (with either continuous or discontinuous fibres). However, such products are not yet commercially available. Adding fibres will result in a highly anisotropic face sheet increasing the in-plane, and out-of-plane stiffness in the 'fibre' dominated direction while keeping the stiffness in the matrix dominated (morphing) direction low. This print strategy can be further exploited to tailor the skin sheets bending stiffness by placing the stiffer TPU phase further away from the neutral axis to increase the bending rigidity [6].

Cellular cores in sandwich panels have been used in aircraft since the 1940s [12] due to their ability to withstand compression and out-of-plane shear loads whilst having a
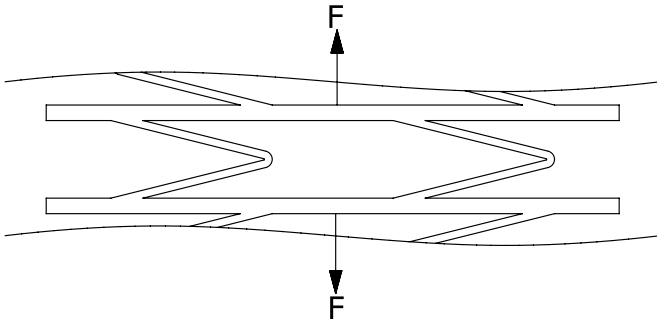
Figure 2. Zero Poisson's ratio cellular MorphCore [16] structure for morphing skins as proposed by Bubert *et al* [17].

Table 1. Core variants.

Panel no.	Skin thickness	Core height
1–9	0.2 mm	6 mm
10–17	0.2 mm	3 mm

low effective density. To further extend the range of achievable mechanical properties, much research over the previous decades has explored alternative geometries to the standard honeycomb shaped cellular core, and it has been shown that Poisson's ratios from $\nu = -1$ to 1 [13–15] can be realised by altering the unit cell geometry.

Zero Poisson's ratio cores are of particular interest in morphing structures, as they allow for large strains in the morphing direction while eliminating the Poisson's effects that would lead to undesired coupled deformations in the non-morphing directions. Because they build up large global deformations through the bending of thin members (with correspondingly low strains), the behaviour of low density cellular solids can be well captured with simple linear elastic analytical methods. The bending elements that make up the cell walls can be modelled as beam or plate elements (with or without shear deformations), as described by Gibson *et al* [18]. Olympio *et al* [19] developed a hybrid honeycomb that exhibits global zero Poisson's ratio properties. It utilises the −ve Poisson's ratio effect found in the auxetic honeycomb and the +ve Poisson's ratio found in the regular honeycomb. The 'MorphCore' [16] (see figure 2), utilised in this work, was developed independently at the same time. It uses a chevron-shaped unit cell with continuous stringers running in the non-morphing direction and thin-walled angled plates which serve as 'bending members'. The bending members provide substantial global deformation capability while the stringers provide the zero Poisson's ratio, as shown in figures 2 and 3.

FFF is the ideal manufacturing process for any core that cannot readily be made using traditional hexagonal honeycomb panels' folding/bending methods. The resulting design freedom afforded by FFF can be used to tailor the core's properties further. For instance, the bending member thickness can be changed to alter the bending behaviour, or flanges can be added to increase the bending stiffness. Adding a second, softer phase TPU can create localised compliant hinges and other features to tailor the core's response for a specific task.

Having laid out the novel GATOR concept, it is necessary to first establish the achievable properties for relatively simple incarnations of the concept before exploring the full range of its design possibilities by carrying out an agnostic analysis of a representative aerospace sandwich panel. The objectives

of this initial experimental study into GATOR morphing skin panels are to evaluate the structural properties of two GATOR skin sandwich panels (3 mm and 6 mm thick respectively, see table 1), which consist of a core covered on both sides by face sheets. Specifically, the in-plane and out-of-plane stiffnesses will be measured as these are the two primary loading conditions of interest for morphing skins. This work also focuses on developing and improving an accurate, reliable and repeatable printing process that these authors introduced in Rivero *et al* [7] will underpin all future work on the concept.

This paper is organised into three sections: first, the panel design approach and its constraints are discussed along with the manufacturing process. Secondly, the methodology and equipment used for the experimental characterisation are presented. Finally, the results of the tests are presented and discussed.

2. Panel design and manufacturing

The panel design and manufacturing were conducted parallel to a preliminary printing trial phase, as the printer hardware and print strategy dictated some parameters. This uses the GATOR design philosophy, which considers the manufacturing process and its advantages and limitations. The panel design and manufacturing are therefore intrinsically linked.

The core is printed from Armadillo (Shore 75D TPU, Fenner Inc. Manheim, USA), a stiffer TPU formulation. The compliant face sheets are printed from NinjaFlex (Shore 85A TPU, Fenner Inc. Manheim, USA), a softer TPU. They are printed as two half panels and then assembled in a second operation. This section looks in more detail at how the bending members and skin thickness were determined and why the panel was manufactured in two halves, which resulted in the panel shown in figure 3.

Bending member: The core's bending member arrangement in figure 3 was chosen to provide a balanced and symmetrical in-plane extension. To get uniform thickness and material properties in the thin bending members, a thickness of 0.6 mm was used. This was dictated by the printer's nozzle diameter print diameter of 0.4 mm to allow at least two nozzle passes. Specifying a thickness slightly less than two full rasters created a small overlap between them, which ensured good bonding between rasters and resulted in a more uniform width.

Membrane thickness: The skin was designed to be made from two layers of material, in total 0.2 mm thick, which is the thinnest membrane that can reliably be printed with the available hardware.

Two piece design: During initial trials, the panels were printed in a single step, with the full height of the core printed directly onto the bottom skin and then the upper skin printed
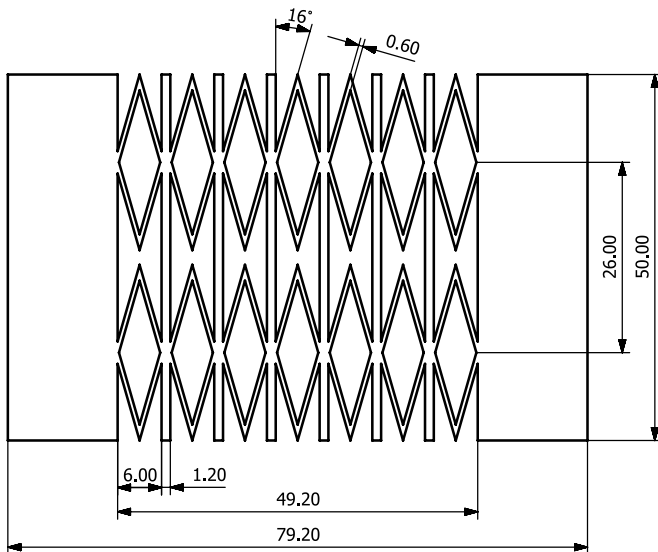
Figure 3. Core design parameters (measurement in mm).

onto the core. While this approach has significant advantages in terms of simplicity and reduced post-processing, it requires the top face sheet to be printed over the open cells of the core, a process referred to as bridging in 3D printing. This negatively affected the integrity of the top face sheet, with skin sagging being observed for unsupported lengths of over 1 mm and incomplete bonding between the two layers making up the top face sheet when gaps greater than 6 mm were bridged. Therefore, it was decided to manufacture the skin in two separate half panels (see figure 4(a)), printing both face sheets directly against the flat printer bed. This then requires a further assembly step of bonding the two halves of the panel, which will be discussed in further detail later (see figure 4(b)).

2.1. Printer hardware and software modifications

FFF 3D printing is a well understood and documented manufacturing method. Nevertheless, it is essential to go into some detail here since the manufacturing process is an integral part of the GATOR concept and printing of flexible materials is deemed to be very challenging. All test panels were FFF 3D printed on a LulzBot Taz 6 equipped with a FlexyDually v2 dual extrusion printer head. This printer head has a dual nozzle and a direct drive system that uses 0.4 mm nozzles. The printer head has two independent drive units, one designed for highly flexible materials and a universal drive for stiffer filament. The printer bed is heated and has automatic self levelling via touch probing at all four corners. Due to their compliance, elastomers are particularly difficult to print and to achieve the print quality desired for this work, the following modifications and procedures were carried out:

- The material feed unit for the Armadillo material was redesigned to reduce the occurrence of material jamming by reducing the internal feed tube diameter. This supports the filament under compression, increasing the driving force that can be applied before filament buckling occurs.

- Both NinjaFlex and Armadillo are hydrophilic and absorb atmospheric moisture over time (Ninjafelx, for example, will absorb 0.22% of its weight in water over 24 h immersed in water, tested to the ASTM D570 standard) [8]. Moisture within the filament will vaporise when heated in the nozzle, causing over extrusion and generating porosity in the printed components. To prevent this, an airtight dry box with silica gel desiccant was used to store the filament, with moisture levels of around ∼10%RH recorded.

- To achieve a uniform membrane thickness and smooth surface, the printer bed had to be adjusted such that the automatic bed levelling offset was as small as possible. Since the printers z-axis is based on a screw drive system, it is expected that there is a small amount of backlash within the lead screw, which caused an uneven print. By manually adjusting the bed so that the software adjustment is minor or not required at all, the skin thickness average variation at printer bed location 1 in figure 5 could be reduced from ±0.021 mm to ±0.013 mm and bed location 2 from ±0.044 mm to ±0.026 mm.

- To improve the surface finish, a PVA coated Kapton tape was stuck to the bed, resulting in a near mirror finish and simplified component removal.

2.2. Settings

Perfectly dialled in print settings are as important as a well adjusted printer to achieve uniform material properties throughout the print.

Due to the compliance of TPU filaments and associated issues with back pressure buildup, they tend to ooze from the nozzle in between periods of extrusion (for example, when travelling or when idle). Nozzle temperature significantly impacts this phenomenon due to the coupling between temperature and viscosity, with higher temperatures causing excessive oozing. On the contrary, if the extrusion temperature is too low, it can cause under-extruded prints or poor layer adhesion. Therefore, it is essential to evaluate the best printing temperature, which may vary depending on environmental conditions and even due to slight variations between batches of material. Once the ideal printing temperature was dialled in, the printer's PID controller was calibrated to avoid any significant temperature drops or overshoots during the print.

The first two layers of the skin panels were printed from NinjaFlex. The extrusion rate was set to 130% to compensate for any fluctuations in pressure within the printer nozzle caused by small changes in height between the nozzle and printer bed. It was found that printed NinjaFlex has high bed adhesion, so much so that it was difficult to remove from the print bed despite using the PVA coated Kapton tape. To reduce the adhesion further, the print speed was increased to 44 mm s^{-1}.

Low inter-layer adhesion was discovered within the core, caused by inadequate time at temperature for complete fusion between layers. This was overcome by raising the nozzle temperature to 218 °C–220 °C (depending on the filament batch) which is the hottest temperature before the nozzle starts to

(a) Single panel as it comes off the printer   (b) Layer by layer view of an assembled panel
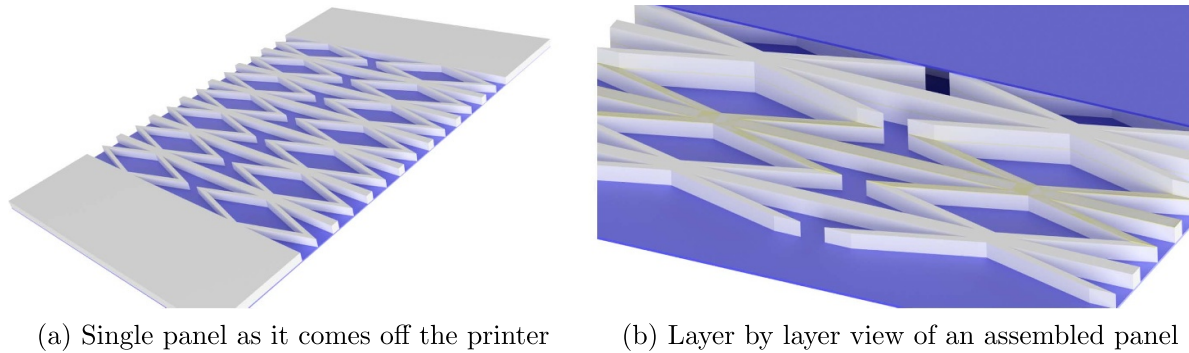
Figure 4. Proposed morphing skin panel made from two different formulation TPU's using FFF manufacturing techniques. Two single panels are bonded together using a two component adhesive illustrated in yellow in (b).
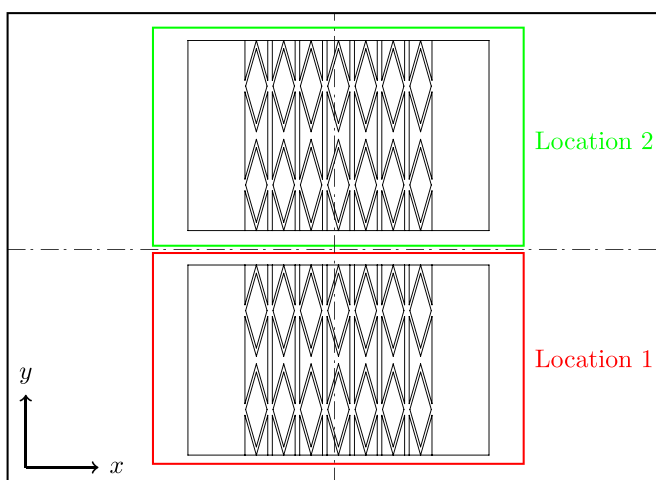

Figure 5. Panel layout on the printer bed centred in *x* and *y* illustrated by the dash-dotted centre line. Note that the print bed is not to scale.

ooze. During the last pass, an ironing cycle was carried out to generate an even and smooth top surface, which reduced the amount of sanding required in the second operation. The final layer was reprinted with an extrusion rate of 10%. A comprehensive list of machine parameters can be found in table 2.

2.3. Panel assembly

Once the two half panels had been printed, they needed to be bonded together to create the full panel specimens. TPUs, being thermoplastic, can be bonded together with adhesives, thermoplastic welding or solvent based bonding, i.e. chemical welding. Adhesive bonding was used in this work since welding large flat surfaces requires specialist equipment, and solvents can be toxic and difficult to apply uniformly. Various types of ethyl cyanoacrylates (superglues) and epoxies were trialled and compared based on their ease of application, bonding strength and cure time. All variants of superglue, despite having excellent bonding strength, caused the NinjaFlex to warp due to chemical interaction with the vapours outgassing

during cure. This outgassing also caused the now sealed cells of the core to pressurise slightly, deforming the face sheets. Ultimately, Araldite 2014–2 epoxy was chosen as it is simple to apply and has a sufficiently long cure time (24 h) to allow for proper alignment and assembly of the panels.

The bonding surfaces on each panel were sanded before assembly to increase mechanical roughness. The components were then cleaned and degreased with Acetone. Once the adhesive was applied, both panels were clamped in an assembly jig to hold them in alignment and provide clamping pressure during the curing process.
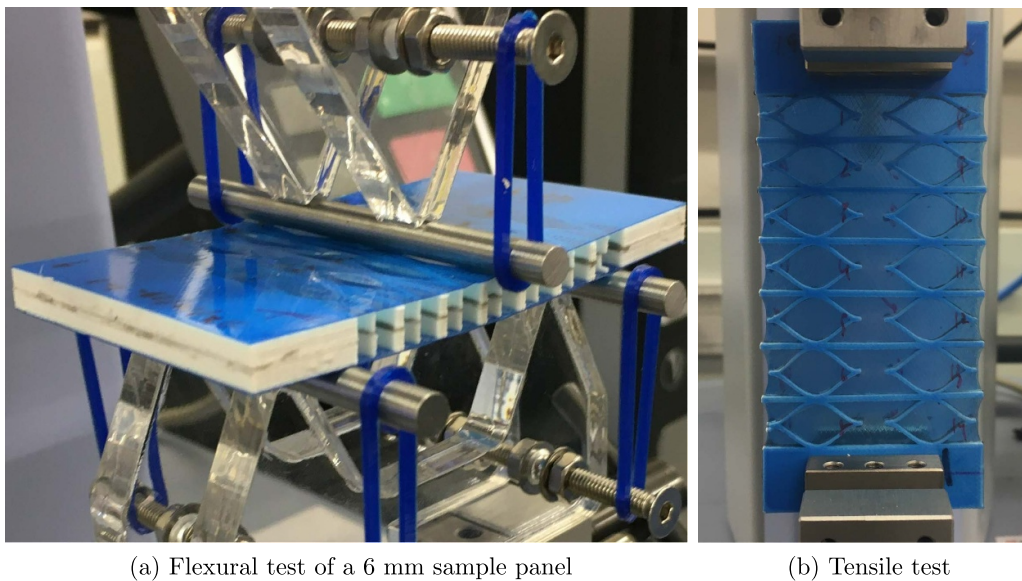
3. Experiment setup

The sandwich panels were tested under three-point bending and tensile loading to determine the out-of-plane and in-plane stiffnesses respectively. There are no established ASTM/ISO test standards specifically for hyperelastic sandwich panels. Still, relevant standards were used in both tests as a baseline, with some modifications required to suit these specimens, as detailed below. All experiments were carried out on a Shimadzu EZ universal test machine with a Shimadzu 2 kN load cell.

The flexural test was carried out following the ASTM D790-17 standard, which describes testing procedures for unreinforced and reinforced plastics. Based on the core design in figure 3, the lower support span was chosen to be 50 mm such that the reinforced end tab (instead of the core) supported the ends of the specimen, as shown in figure 6(a). A bespoke test fixture was designed following the above mentioned standard. Detailed displacement measurements along the length of the panel were captured using a video gauge, which tracked a series of black dots painted on the panel members shown in figures 6(a) and 7. All experiments were carried out with a crosshead motion rate of 0.6 mm min^{-1} with an overall crosshead displacement of 12 mm. All panels were tested for their flexural properties in both directions by flipping them over and repeating the test.

Following the flexural tests, the specimens were tensile tested to a stretch ratio (which is denoted by λ) of $\lambda = 1.6$, where the stretch ratio is defined as the ratio between the final

5

Table 2. Optimised print parameters for NinjaFlex and Armadillo determined from dedicated calibration- as well as test prints.

		Material	
Value	Description	NinjaFlex	Armadillo
Feed rate (mm s^{-1})	Initial layer	44	35
	Final layer	35	35
Extrusion temperatures (°C)	Initial layer	245	218–220
	Final layer	240	218–220
Extrusion rate (%)	Initial layer	130	100
	Final layer	105	100
Layer height (mm)		0.1	
Wall layers		3	
Infill raster orientation (°)		[45, −45]	
Print bed temperature (°C)		25	

(a) Flexural test of a 6 mm sample panel

(b) Tensile test

Figure 6. Experimental test setup. Where (a) is a panel at the point just after buckling and (b) a panel at $\lambda = 1.6$.
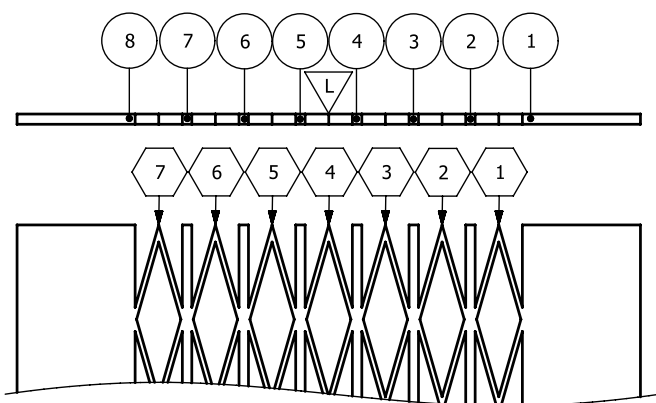
Figure 7. Representation of the displacement measuring points (in circles) and unit cell row (in hexagon) numbering system. 'L' denotes the position where the load is applied.

length and the initial length of the active portion of the specimen (excluding end tabs). This value was chosen as it is just below the manufacturer's specified yield point of $\lambda = 1.65$ for NinjaFlex [8]. The maximum stretch was driven by the face

sheets and not the core because the Armadillo core sees much lower local strains, and the material yield point of $\lambda = 1.18$ was not approached. It was decided to base the tensile tests on the ISO 527-1:2019 standard for determining the properties of plastics. However, the specimen dimensions were driven by the flexural testing standard and not any tensile test standard. This is the same standard Reppel *et al* [11] used when testing NinjaFlex monolithic dogbone test specimens in uniaxial tension. The crosshead displacement rate was set to 1 mm s^{-1}, and the specimens were cycled three times. All specimens were clamped on the endtab section, as shown in figure 6(b).

4. Results and discussion

4.1. Overall manufacturing accuracy and print quality

Each panel was carefully measured for its dimensions and manufacturing accuracy to quantify the variance. The skin and member thickness were measured before assembly and the overall height after assembly.

4.1.1. Visual inspection. All panels were visually inspected for any imperfections or damage from the removal from the print bed. The interface between the skin and the core was a particular area of interest, ensuring a strong bond between the two materials. No layer separation was detected, and the skin was firmly bonded to the core. This was later confirmed during tensile testing when it was found that the skin remained firmly attached. Overall all panels were of satisfactory visual standard.

4.1.2. Skin thickness. The skin thickness was measured in the centre of each unit cell with a calibrated spring loaded constant pressure micrometre (Hummel Cie., Solothurn, Switzerland, measuring resolution $\pm 1\,\mu$m). Whilst great care was taken in taking the thickness measurements, and best practices in measuring hyperelastic materials were followed [20], some variation in the skin thickness can be caused by the local compression during the contact measuring process. Using a constant pressure micrometre can reduce this error considerably. It was found that there is some thickness variation, as shown in figure 8(a). This is partly influenced by the location on the print bed a given specimen was made and the automatic bed levelling. It was found that the bed in position 1 is flatter which is indicated by the error bars in figure 8(a). The nozzle cleanliness can severely influence the automatic bed levelling, which works by closing an electrical circuit between the nozzle and the print bed corners. Any plastic on the nozzle acts as an insulator which causes a delayed response by the printer. The nozzle was therefore cleaned before each print to minimise this effect.

4.1.3. Bending member thickness. The bending member thickness was measured using calibrated high precision vernier callipers (Tesa SA, Bienne, Switzerland, measuring resolution $\pm 5\,\mu$m). As shown in figure 8(b), there is a significant variation within the bending member thickness, higher than seen in the skin thickness. The error source was identified as the *x* and *y*-axis drives, specifically backlash within the drives belt/pulley interfaces. This issue is exacerbated in the printer used due to a particularly heavy print head cantilevered off the *y*-axis drive mechanism. The backlash issue was not readily addressable as it is a printer specific feature but was consistent for all the specimens tested.
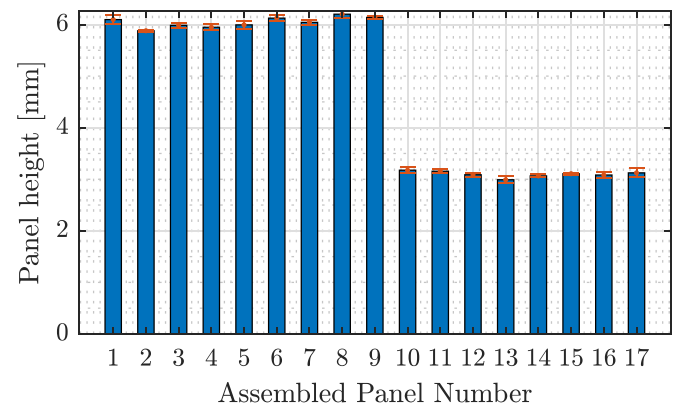
4.1.4. Panel height. The overall height of the panels was measured using a constant torque micrometre which was also used for measuring the skin thickness. The measurements in figure 8(c) show that using an adhesive does not have a negative impact on the accuracy of the final dimensions as there is only a small amount of variation present. Panels used in specimens 1, 4, 5, 13 and 17 had a rougher bonding surface finish after printing when compared against the others due to variations in the surface ironing process. Therefore more sanding was required before bonding which may have impacted the dimensional accuracy.
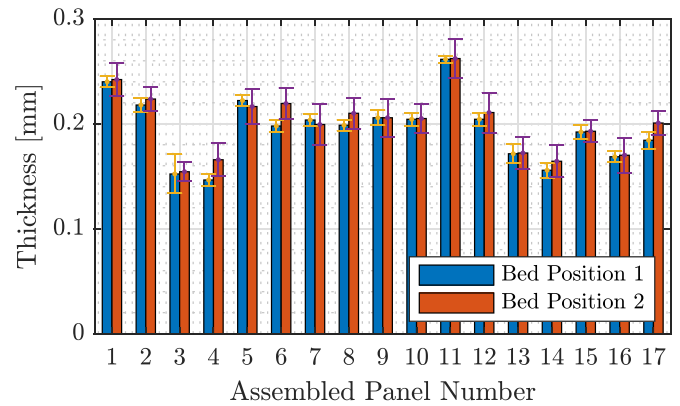
(a) Skin thickness
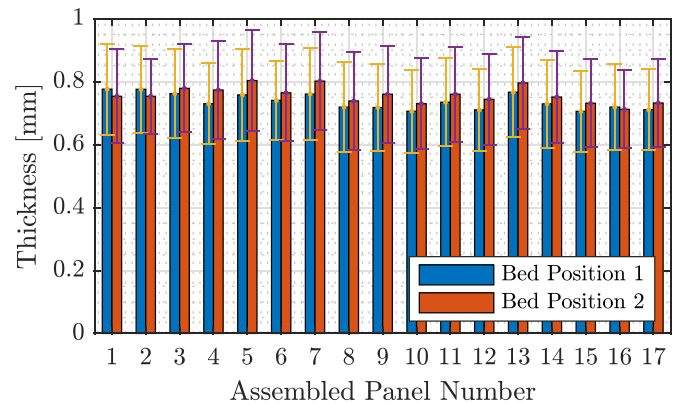
(b) Bending member thickness

(c) Overall assembled panel height

Figure 8. Measurements of skin and core bending member thicknesses and the overall assembled height of each panel. The skin and member thickness are separated based on where on the printer they were made, where position 1 is to the front, and 2 is at the back.

4.2. Impact of the dimensional accuracy on the overall structural behaviour

All dimensions discussed in this section will impact the structural performance. However, skin stiffness, directly linked to skin thickness, is the driving factor in the in-plane mechanical response. At the same time, the out-of-plane performance is dominated predominantly by skin thickness and core height. On the other hand, the bending member mean thickness
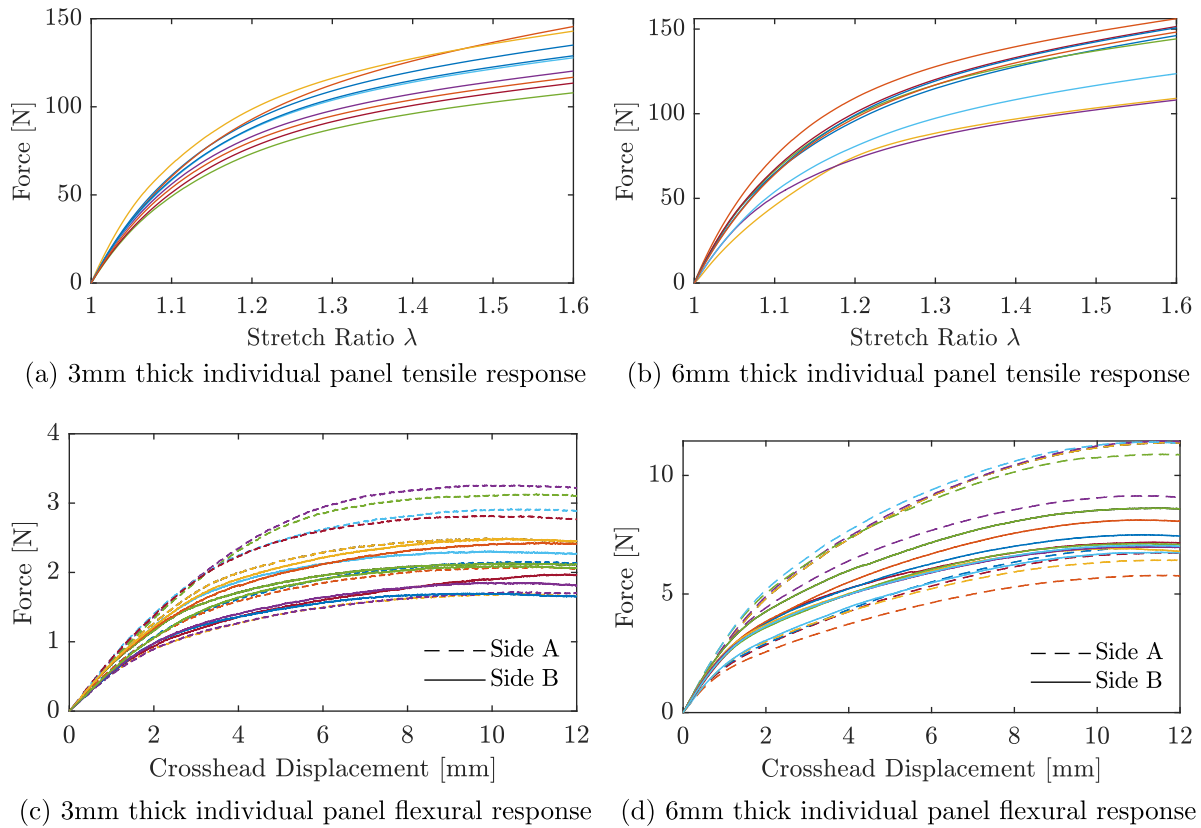
(a) 3mm thick individual panel tensile response

(b) 6mm thick individual panel tensile response

(c) 3mm thick individual panel flexural response

(d) 6mm thick individual panel flexural response

Figure 9. The individual responses of each panel both for the tensile as well as flexural loading case where the responses in (c) and (d) are distinguished between sides A and B.

of 0.750 mm would lead to a minimally increased in-plane stiffness variation across a core, resulting in an uneven bending of the bending members. This does not seem to impact if we compare core only performance with each other. Figure 13, which we will discuss later in more detail, shows that there is minimal variation in response between the individual specimens printed with the same printer and parameters outlined earlier and the same dimensional variation.

4.3. Tensile test

The variation in response between the individual panels in both the tensile and flexural loading conditions turned out to be large, as shown in figure 9, which is expected testing components made from hyperelastic materials. The ISO 37 standard for testing tensile properties of rubber and thermoplastic elastomer suggests using five or more samples to take an average of a data set due to the variation between each sample. Based on this, all data will be presented with the mean response from all panels and a shaded area representing the range for better clarity.

Panels 1–6 were tested to find the limit load, effects of extension rate and yield point. The remaining panels were used for cyclic load testing and cycled three or ten times. The dwell time between each cycle was chosen to be zero to represent the cyclic loading experienced on an aircraft and allow as little

relaxation as possible. Cyclic testing showed a strong load history dependency, with an apparent hysteresis expected for hyperelastic materials (see figure 10(a)). It was also found that all samples, independent of the core height, showed a considerably different loading response during the first cycle compared with the remaining cycles (see figures 10(b) and (c)).

The measured tensile response during both the first and second cycle generally matches what would be expected for hyperelastic materials, although there are some interesting features. Comparing the averages between the first cycle in figure 10(b) and the second cycle in figure 10(c) respectively, it can be seen that there is a stiffening non-linearity at high stretch ratios during the second cycle, which was also seen in subsequent loading cycles. This can also be seen in figure 10(a). In the first cycle, no such effect is evident; in fact, softening is found as the λ tends towards the maximum ($\lambda = 1.6$). The panels were measured before and three weeks after testing to allow them to ensure maximum relaxation since all panels were found to be stretched upon unloading from the tensile tester. None of the panels tested during cyclic testing showed visible nor measurable signs of permanent deformation, where the measurements were taken three weeks after testing to allow sufficient relaxation.
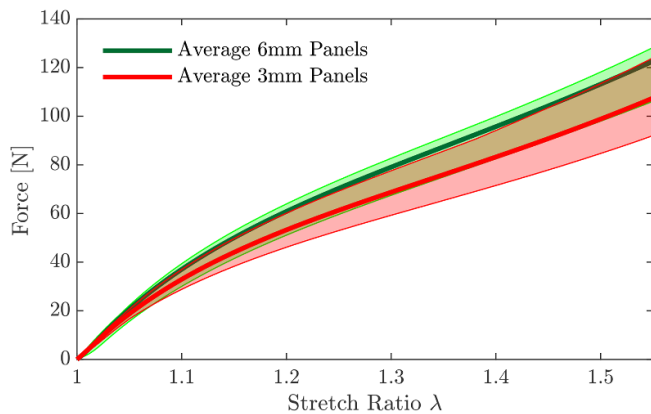
Panel 3 was tested too much larger stretch ratios to explore the failure mechanisms. The first drop in force was detected at $\lambda = 2.75$ and a load of 359.4 N, where the two panel
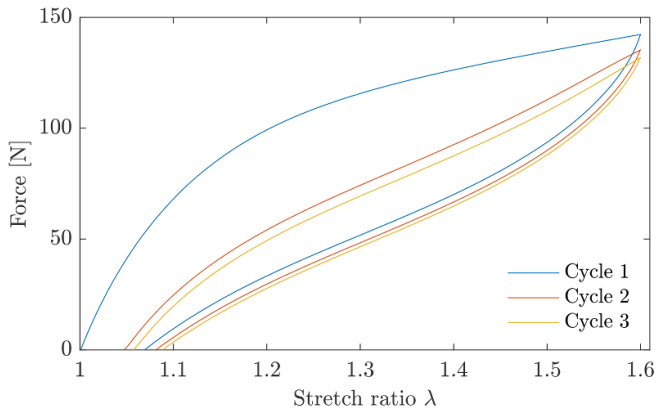
(a) Three load cycles for a 3 mm thick panel (panel 10)
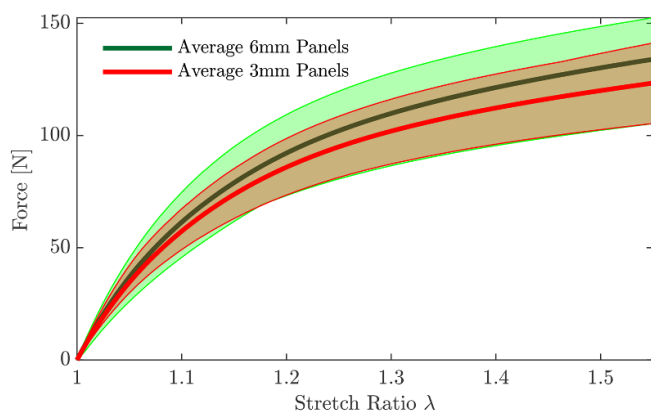
(b) First load cycle for all panels (Note: The shaded area represents the data range)

(c) Second load cycle for all panels (Note: The shaded area represents the data range)

Figure 10. Tensile loading of the 3 mm and 6 mm specimens.

halves separated at the corner of one of the bending members due to adhesive failure at the row closest to the grip. The skin remained firmly attached to the core until the fracture of the bending members at $\lambda = 2.97$ and a load on 392.8 N, where it only separated at the row of unit cells that failed.
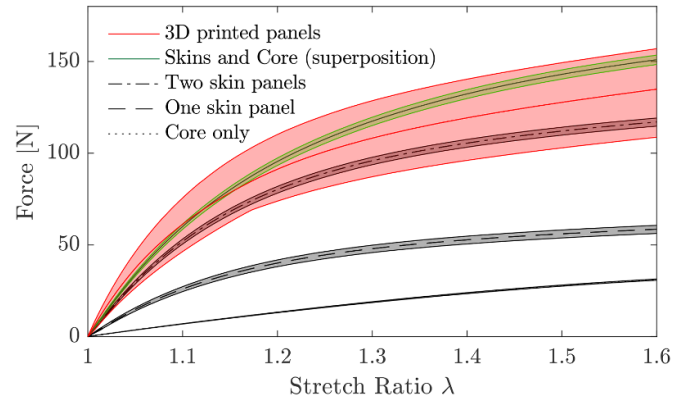
Figure 11. Tensile test data show components and total response. The green area represents the assumption that the panel's response is a linear superposition of the core and skin component responses (no interaction effects). The results in red are for the assembled 6 mm panels.

This corresponds with the finding of these authors where a skin sheet printed onto Armadillo tabs was taken to failure, and no separation was detected [7]. Panel 2 was taken to a stretch ratio of $\lambda = 1.8$, at which permanent deformation was expected. In the direction of pull, the panel was permanently deformed by 3.9% (measured three weeks after the experiment).

4.4. Tensile testing of core and skin components

The core and skins were also tensile tested as separate components to better understand their behaviour. Bubert *et al* [17] showed that this particular MorphCore configuration exhibits a linear behaviour up to a stretch ratio of $\lambda = 1.3$. However, it was unknown whether there are any non-linear responses at larger deflections as seen in hexagonal honeycombs [21] and in combination with the non-linear material properties of TPU.

It was found that the core exhibited a relatively linear response as shown in figure 11 up to a stretch ratio of $\lambda = 1.6$ to which all specimens were tested. It can also be observed that the cores show a low variation between specimens. The individually tested skin sheets showed a highly non-linear response—with a noticeable softening effect above a stretch ratio of roughly $\lambda = 1.1$. The overall curve shape in figure 11 is similar to the one compared with a fully assembled panel, implying that the skin sheets primarily drive the overall panel response. To prove that the skin sheet governs the overall panel response, experimental data from the 6 mm core panels were compared against an artificial panel result composed of a linear superposition of the individual skin and core responses. Both the skin and core model and the fully 3D printed specimens show more or less a similar response. At stretch ratios greater than $\lambda = 1.1$ a divergence of the superposition result from the fully 3D printed specimens can be observed—making it stiffer than the sandwich panel. The difference suggests that there is some interaction between the core and the skin that a model by superposition is not able to capture—particularly at large
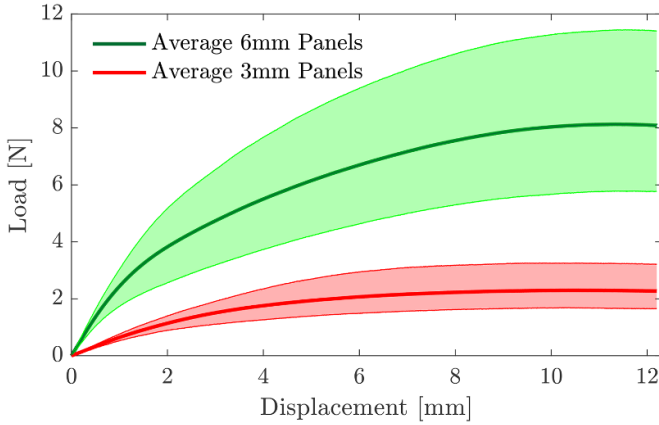
Figure 12. Three point bending test response ranges and averages for the 3 mm and 6 mm panels.

Figure 13. Flexural test data show components and total panel response for a 6 mm thick panel. The core and full panel responses were measured directly, while the skin's contribution was estimated using the approach described in the text.

stretch ratios where it is likely that the skin enters a non-linear behaviour sooner, resulting in softening of the overall panel. The skin/core interaction will be explored in more detail in future work.

4.5. Three point bending tests

All panels were tested for their flexural response as described above. The experiments were carried out on both sides of the panels to determine whether there is any difference due to the direction of loading, with the differences in skin thickness being one potential source of difference. To allow the panels to relax from the flexural test, all specimens were tested on one side first, then on the other. It was initially found that the panels would interact with the bottom support rollers due to the softness and high friction of Ninjaflex skin, leading to a stick-slip phenomenon. This was mitigated by covering the end tabs with a layer of Kapton tape.

A highly non-linear response was found in the flexural data for both the 3 and 6 mm panels, along with a significant variance in the measured forces. This is illustrated in figure 12 where the solid lines represent the average response of all panels tested and the shaded area the spread of results. It can be observed that there is at first a relatively linear behaviour in both the 3 and 6 mm specimens up to about $\sim$0.75 N and $\sim$1.8 N respectively before they start to behave in a non-linear fashion. This softening behaviour occurs after roughly $\sim$1 mm of displacement in both cases, which for an active length of 50 mm represents a normalised displacement of about 2% of length. For a morphing application, these skin panels would most likely be designed to deform less than 2% under load to avoid adverse aerodynamic effects due to aerofoil geometry changes, which indicates that this softening nonlinearity may not very well be a relevant feature in use.

Of primary importance here is the impact that the use of a sandwich structure has on the out-of-plane stiffness of the panels, as this is the reason for their design. This can be seen by considering the difference in bending stiffness between the
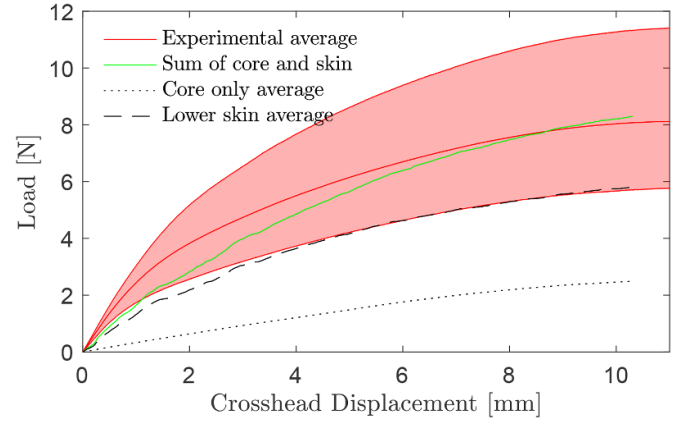
core by itself and the assembled panels. Figure 13 shows the thicker panel's response compared to the core by itself. It is worth noting that the bending stiffness of the $\sim$0.2 mm face sheets by themselves is so low as to be untestable with this setup—they can not even support their own weight enough to stay on the rollers. The 6 mm core also has low inherent stiffness, with an initial stiffness of $\sim$337.2 N m^{-1}. The assembled panel on the other hand has an initial linear stiffness of $\sim$2789.8 N m^{-1}, which represents a very significant 727% increase over the core by itself (and an even more significant gain over the skin by itself). As expected due to the non-linear impact of the thickness of bending stiffness, the 3 mm panel has significantly less than half the stiffness of the 6 mm panel, with an initial linear stiffness of $\sim$658.6 N m^{-1}, which is only 24% of the 6 mm panel result.

Further insight can be gained by considering the effective bending and axial rigidity of the different tested structures and their mass properties. While the deformations of the structures under load are complex, it is useful to consider an equivalent bending rigidity of EI_{eq} and axial rigidity of EA_{eq} as a first order representation of their inherent bending and axial behaviour. This is done using simple beam theory in the linear regime of specimen response to solve for the equivalent rigidity that would produce the same force vs crosshead displacement responses. Equations (1) and (2) show the Euler-Bernoulli beam bending and linear axial stiffness equations, respectively, that were used where F denotes force at the load cell, L_{EI} the distance between the three-point test support, L_{EA} the core initial length and δ the crosshead displacement.

$$EI = \frac{F L_{EI}^3}{48\delta} \tag{1}$$

$$EA = \frac{F L_{EA}}{\delta}. \tag{2}$$

Table 3. 3 mm and 6 mm core-skin panels, 6 mm core and skin only comparison metrics.

	Panel (3 mm)	Panel (6 mm)	Core (6 mm)	Face sheet
Mass[c] (g)	9.154[a]	17.137[a]	15.885[a]	0.801
Mass Standard Deviation	0.3141	0.3269	0.0551	0.1143
EA (N)	873.658	816.751	80.005	303.956
EI ($\times 10^{-3}$) (Nm^2)	1.715	7.265	0.878	0.001 01[b]
EI/EA ($\times 10^{-6}$) (m^2)	1.968	8.393	10.976	0.003 33
EA/Mass (Ng^{-1})	95.192[a]	50.511[a]	5.037[a]	379.957
EI/Mass ($\times 10^{-3}$) (Nm^{2}g^{-1})	0.187[a]	0.424[a]	0.0553[a]	0.001 27[b]
EI/EA/Mass ($\times 10^{-6}$) (m^{2}g^{-1})	0.215[a]	0.490[a]	0.691[a]	0.004 17[b]

[a] This includes mass of the end-tab used to clamp the specimen in the tensile tester.
[b] EI is calculated using E obtained experimentally and I is calculated from the mean skin dimensions.
[c] Weighed on Mettler-Toledo MS-TS scales.

The average values of these rigidity values are shown in table 3, along with specimen masses and several comparison metrics. We see here that moving from the 6 mm core to the 6 mm panel yields a 727% increase in bending rigidity for a 7.9% increase in mass, where the mass added also serves the vital function of creating the continuous, sealed skin surface.

Comparing the 3 mm panel to the 6 mm, it can be seen that the 324% increase in rigidity requires only an 87% increase in mass—showing the highly non-linear benefits of sandwich panel core height. This is seen as a 453% increase in the mass-normalised bending rigidity. While the skin could not be directly tested in bending, we can still make a meaningful comparison by considering how thick and heavy a solid skin sheet of the softer TPU would have to be to match the bending rigidity of the 6 mm panel. For this, we approximate the EI using the experimentally measured initial linear elastic tensile modulus ($E = 30.4$ MPa) and basic geometry to estimate the second moment of area as that of a solid rectangle. This solid skin would be 1049% heavier than the panels tested here, which are not even mass optimised.

Since the competing constraints of morphing skins are low in-plane stiffness and high out-of-plane stiffness, the motivation for using GATOR skins can be seen if we consider the ratio of bending to axial rigidity in the rigidity ratio EI/EA. This metric effectively captures the fundamental design trade off inherent to these structures and highlights the advantages of the GATOR skins. Dividing this metric by panel mass allows this additional design driver to be included into a mass-normalised rigidity ratio. Here a comparison between options is even starker. Solid elastomeric skins are very poor performers compared to sandwich panels, with the 6 mm panel provides a 2520 × increase in rigidity ratio and a 120 × increase in mass-normalised rigidity ratio. These results clearly show the effectiveness of the core underlying principles of the GATOR concept.

After the initial linear portion of response (on which the above discussion is based), the loading in the panel because asymmetric through the thickness as the upper skin sheet is in

compression, but due to its thinness and low material stiffness, it undergoes a form of local panel buckling in between the stringers of the core (see figure 14). Therefore, only the core and lower (tension) skin contribute significantly to the flexural stiffness at higher load levels.

To investigate this further, let us look at how the panels respond if the upper skin cannot take any compression and, as a result, buckles immediately upon applying a load which we modelled by ignoring the skin in compression altogether. To make this comparable to the response of the fully 3D printed panels, experimental data from core and skin only flexural tests (see figure 14) were used. In this test, the skin strains were not directly measured. So they were instead calculated for each unit cell using the video gauge tracking information and the experimental face sheet data set from the *EA* tests to represent the face sheet's non-linear behaviour. They were analysing the video tracking data, it was found that the nodes moved closer together throughout the loading cycle, as illustrated in figure 15. This effect was used to calculate the skin strain given the distance from the neutral axis, assuming that the neutral axis forms a perfectly circular arch and that there is no axial compression within the core and no interaction between the skin and core and vice versa. A core without skin sheets was tested to get the core only response.

A highly non-linear response can be observed comparing the single skin model representing the post-buckling condition with a 6 mm fully 3D printed panel in figure 13. Initially, the full panel results are significantly stiffer than the estimated core plus tension skin only panel, indicating the compression skin is contributing significantly. As displacement increases, however, the full panel softens earlier, and its force response approaches that of the single skin. This helps to support the observation that the top, compressive skin sheet can contribute significantly to the overall bending stiffness only up until the point it buckles. It is important to note, that these sandwich panels are at their resting length, and therefore they do not benefit from the buckling delaying benefits that axial extension of the panel (either pre-tension or morphing induced deformation) would introduce.
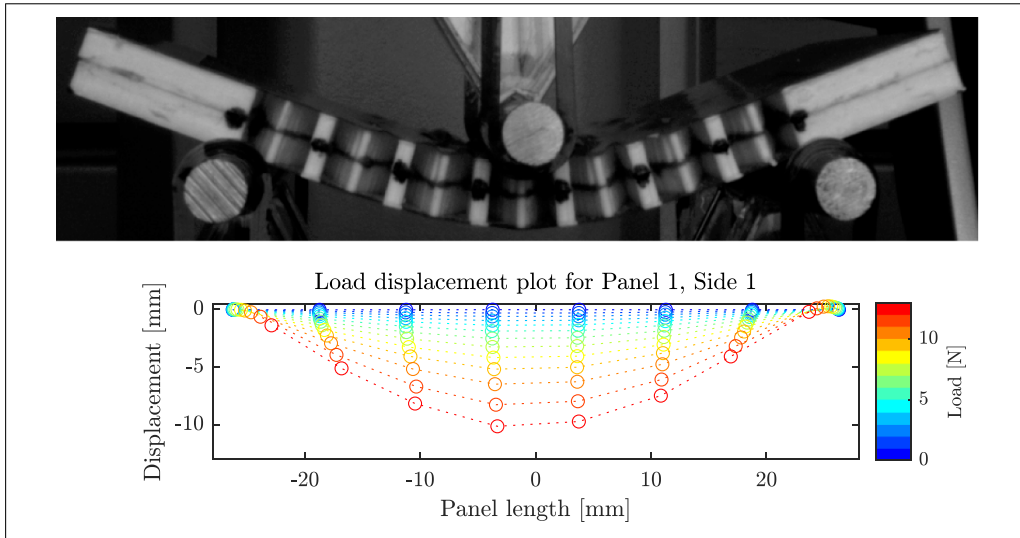
(a) 6 mm panel.
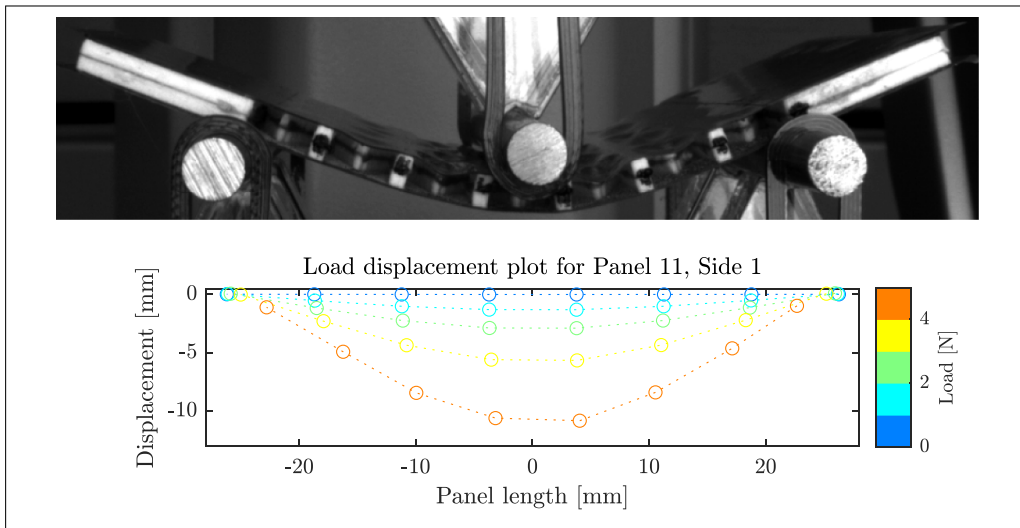
(b) 3 mm panel

Figure 14. Displacement distribution plots show variation in displacement along panel length for different load levels past the point of buckling. The photos above show the panels at a displacement of 6 mm.
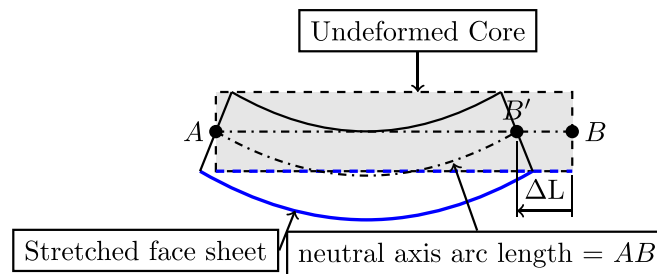

Figure 15. Assumed unit cell deformation mechanism through the panel's neutral axis. Points A, B and B' represent tracking points on the core (as shown in figure 7). AB is the length of an undeformed cell and AB' is a deformed unit cell.

5. Conclusions

The aim of this paper was to 3D print and characterised GATOR morphing skin panels to develop the manufacturing method further and to show the achievable performance. While the GATOR concept covers a wide range of potential skin configurations, these initial proof-of-concept specimens consisted of simple sandwich panels made from a zero Poisson's ratio

core covered with flexible face sheets. Both the skin and the core were printed in the same process using two different formulations of TPU. The printed specimens were tested for their in-plane and out-of-plane flexural properties. The following conclusions can be drawn:

(a) The promising printing results in this research show that different formulations of TPU can be reliably printed in a single operation into fully functioning GATOR skin panels. It has discussed the key manufacturing process settings that dictate the quality of the manufactured articles. One remaining process limitation is the significant variation in dimensions across the bending members. This is not anything intrinsic to the concept and could be directly improved with better hardware.

(b) A strong bond between the softer skin phase TPU and the stiffer core was achieved *in situ* during the printing process, requiring no further modification.

(c) This paper has shown that the MorphCore's in-plane behaviour over considerable deflections up to a stretch ratio $\lambda = 1.6$ is mainly linear. The in-plane response of the full sandwich panels was found to correlate well with a linear superposition of the different elements composing it. However, differences exist, which may be better explained through future research focused on interaction effects.

(d) The flexural results show that the top skin sheet can resist a small amount of compressive loading without buckling, resulting in a linear behaviour at the small to moderate displacements that would be expected in an application—even without any form of skin tensioning.

(e) The underlying scaling laws that the GATOR concept seeks to exploit were shown directly: doubling the core height from 3 mm to 6 mm gives a 727% increase in bending rigidity with a mass increase of only 7.9%.

In summary, this work has provided insight into the potential efficacy of the GATOR skin concept in helping to address the competing design constraints faced by morphing skins. Very high in-plane deformations were achieved at modest actuation force, and the out-of-plane stiffness was found to scale favourably due to the multi-material sandwich panel approach. The manufacturing method has produced good quality, repeatable, robust components. Future work will implement more complex GATOR skin configurations and explore the achievable design space more thoroughly using analytical, numerical, and experimental methods.

Data availability statement

All data that support the findings of this study are included within the article (and any supplementary files).

ORCID iD

Rafael M Heeb https://orcid.org/0000-0001-7834-3650

References

[1] ICAO 2019 ICAO environmental report 2019: destination green: the next chapter *Technical Report* (Montreal: ICAO)
[2] Yokozeki T, Takeda S I, Ogasawara T and Ishikawa T 2006 *Composites* A **37** 1578–86
[3] Bartley-Cho J D, Wang D P, Martin C A, Kudva J N and West M N 2004 *J. Intell. Mater. Syst. Struct.* **15** 279–91
[4] Wilson T, Kirk J, Hobday J and Castrichini A 2019 IFASD 2019 International forum on aeroelasticity and structural dynamics 2019
[5] Gandhi F and Anusonti-Inthra P 2008 *Smart Mater. Struct.* **17** 015025
[6] Woods B K and Heeb R M 2021 *J. Intell. Mater. Syst. Struct.* (https://doi.org//10.1177/1045389X221096155)
[7] Rivero A E, Fournier S, Heeb R M and Woods B K 2022 *Appl. Sci.* **652** 2–19
[8] NinjaTek 2016 NinjaFlex 3D printing filament *Technical Report* (NinjaTek)
[9] Recreus 2017 FilaFlex *Technical Report* (Recreus Industries, S.L.)
[10] Polymaker 2015 PolyFlex technical data sheet *Technical Report* (Shanghai: Ployflex)
[11] Reppel T and Weinberg K 2018 *Tech. Mech.* **38** 104–12
[12] Cutler J 2005 *Understandig Aircraft Structures* (Oxford: Blackwell)
[13] Masters I G and Evans K E 1996 *Compos. Struct.* **35** 403–22
[14] Prall D and Lakes R 1997 *Int. J. Mech. Sci.* **39** 305–14
[15] Hoffman G A 1958 *J. Aerosp. Sci.* **25** 534–5
[16] Kothera C S, Woods B K S, Wereley N M, Chen P C and Bubert E A 2007 Cellular support structures used for controlled actuation of fluid contact surfaces *United States US7931240B2* (available at: https://patents.google.com/patent/US7931240B2/en)
[17] Bubert E A, Woods B K, Lee K, Kothera C S and Wereley N M 2010 *J. Intell. Mater. Syst. Struct.* **21** 1699–717
[18] Gibson L J and Ashby M F 2014 *Cellular Solids: Structure and Properties* 2nd ed (Cambridge: Cambridge University Press)
[19] Olympio K and Gandhi F 2007 Zero-v cellular honeycomb flexible skins for one-dimensional wing morphing *15th Structural Dynamics and Materials Conf.* (Honolulu, HI: AIAA/ASME/ASCE/AHS/ASC Structures) pp 1–28
[20] Brown R 2018 *Physical Test Methods for Elastomers* 1st edn (Cham: Springer Nature)
[21] Gibson L J 1981 The elastic and plastic behaviour of cellular materials *PhD Thesis* University of Cambridge, Cambridge